BULLETIN OF THE POLISH ACADEMY OF SCIENCES
TECHNICAL SCIENCES
Vol. 55, No. 3, 2007

An integrated inverter for a single-phase single-stage grid-connected PV system based on Z-source

Z. CHEN, X. ZHANG, and J. PAN*

Department of Electrical Engineering, Shanhai Jiao Tong University, Shanghai 200030, P.R.China

Abstract. An integrated Z-source inverter for the single-phase single-stage grid-connected photovoltaic system is proposed in this paper. The inverter integrates three functional blocks including maximum-power-point-tracking, step-up/down DC-side voltage and output grid-connected current. According to the non-minimum-phase characteristic presented in DC-side and the functional demands of the system, two constant-frequency sliding-mode controllers with integral compensation are proposed to guarantee the system robustness. By using two controllers, the effects caused by the non-minimum-phase characteristic are mitigated. Under the circumstance of that the input voltage or the grid-connected current changes suddenly, the notches/protrusions following the over-shoot/under-shoot of the DC-bus voltage are eliminated. The quality of grid-connected current is ensured. Also, a small-signal modelling method is employed to analyze the close-loop system. A 300W prototype is built in the laboratory. A solar-array simulator (SAS) is used to verify the systematic responses in the experiment. The correctness and validity of the inverter and proposed control algorithm are proved by simulation and experimental results.

Key words: Z-source inverter, single-phase single-stage grid-connected photovoltaic system, sliding-mode controller.

1. Introduction

In the 90's of the last century, the centralized mode is used in the photovoltaic (PV) system. Many parallel solar cell arrays (SCAs) connect the grid by using one inverter. Recently, the decentralized technology that each PV module is less than 500W has been put into use in PV systems [1-3].The technology enhances the flexibility and expansibility of PV grid-connected systems.

Most of actual PV grid-connected systems consider only the static characters of the SCAs, not the dynamic stability. In fact, when the irradiance amplitude changes rapidly, especially the irradiance decreases suddenly, the working point of the output voltage and current of the SCAs will be changed simultaneously, and the voltage amplitude will decrease in a sudden manner, which will maybe cause the DC-bus voltage to collapse. The dynamic stability of the PV system in the case of the sudden changes has been studied, and the model of the SCAs is established based on the experimental results [4]. Dr. Wu analyzed the collapse process of the DC-bus voltage in the single-stage PV grid-connected system and proposed a vary-step MPPT method [5]. But even if the method is put into use, the collapse still exists and its range is dependent on the value of the step and the sample-cycle of the MPPT method. Furthermore, in the traditional single-stage system the voltage of the solar-cell must be greater than the peak of the grid voltage to ensure the grid-connected success.

The Z-source inverter is a new inverter proposed in 2003 [6]. An impedance-source (Z-source) is used to replace the DC-bus capacitance or inductance so as to overcome the limitations of the traditional inverters that voltage amplitude can only be boosted or bucked. At the same time, the Z-source network has good flexibilities because its main circuit may be either the voltage-source or the current-source, so the inverter bridge can be permitted to short or open. The Z-source inverter has been used widely in many realms [6-8].

The transfer function of the Z-source impedance has a right-hand-plane (RHP) zero which can't be eliminated by adjusting the parameters [9,10]. The unstable zero brings an obvious over-shoot and a following notch because of the energy resettling when the input voltage declines rapidly [11]. Many literatures have been focused on the disadvantages. A discrete-time PI controller is used to control the voltage of Z-source capacitors under the circumstances of the slow change of input voltage [12]. A multi-loop closed loop controller is proposed to minimize the effects of non-minimum phase characteristics. But when the input voltage declined suddenly an over-shoot and a following notch of the DC-bus voltage still exists obviously due to the bandwidth limitation of the proposed controller [11], and recovering time to zero state error is about 40ms.

This paper presents an integrated single-phase single-stage PV grid-connected inverter based on the Z-source. The inverter has three functional blocks, namely maximum power point tracking (MPPT), voltage boost and current output according to the grid-connected standards. In the proposed system, the constant switching frequency is

* e-mail: chen.zongxiang@gmail.com

needed because the above-mentioned three functional blocks are realized by controlling four power-switch devices of the inverter bridge logically. Considering the dynamic characteristics of the SCAs, the non-minimum-phase characteristics exhibited in the DC side, the quality of the grid-connected current and the constant-frequency demands, two constant-frequency sliding-mode controllers (SMCs) with the integral compensation based on variable structure theory is proposed in this paper. Usually the reference part is a constant value and its derivative is zero. So the error items can be replaced by state variables in the controllers. In order to use the equivalent control of the SMC directly as the duty cycle control, the integral component of the references' error is introduced to make its derivative still contain reference information. It can also track the error in the sliding surface to ensure the static-state and dynamic performance of the system [13, 14]. In the sliding mode, the system can't be influenced by the change of systematic parameters and the disturbances. It has strengthened the self-adaptability and robustness. Via the DC-side controller the fast recovery with zero steady-state error is exhibited when the perturbations of the input voltage occur. Especially the following notch/protrusion is eliminated even if the input voltage declines/rises abruptly. Besides, when the grid-connected current decreases/increases rapidly, the DC-side voltage isn't impacted. The over-shoot/under-shoot of the Z-source-network output voltage doesn't appear. All of these control results ensure the quality of the grid-connected current. Furthermore, a small-signal modelling method is employed to analyze the close-loop system to prove the system stability. A 300W prototype is built in the laboratory. A solar-array simulator (SAS) is used to verify the systematic responses in the experiment. The correctness of the integrated PV grid-connected inverter and the validity of the proposed control algorithm are proved by the simulation and experimental results in this paper.

2. Operating principle of the single-phase integrated inverter with Z-source

The structure of single-phase PV grid-connected inverter is shown in Fig. 1.

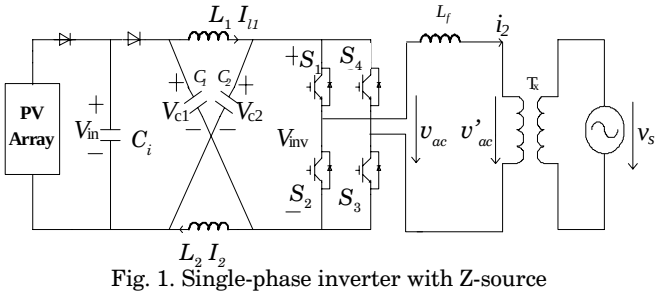

Fig. 1. Single-phase inverter with Z-source

Comparing the Z-source inverters with the traditional ones, a shoot-through state that the upper and lower switch devices of any one phase leg are shorten is added besides the zero state and active state. This is the best advantage and feature of the Z-source. Some special switch logical relation must be obeyed, because all the functional blocks, including MPPT, voltage boost and current output, are realized by controlling four devices of the inverter bridge. The two switches of one phase leg cannot be closed simultaneously while the inverter outputs the current to the grid in order to ensure the quality of the grid-connected current. On the contrary, the grid-connected current cannot be output while the two switches of one phase leg are working in the shoot-through state.

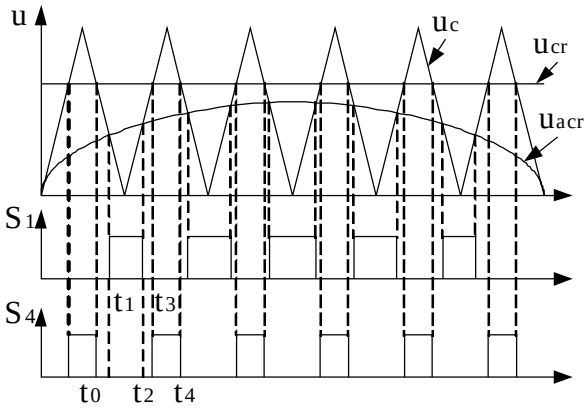

Fig. 2. The Z-source inverter control mode (positive or negative cycle)

A unipolar control method is used in the paper [15]. Taking the positive half-cycle, its basic switching mode is shown in Fig. 2, where u_{acr} is an AC-current modulation signal, u_{cr} is a DC-voltage modulation signal to be used to boost DC voltage as desired, and u_c is a carrier signal. From Fig. 2, when the instantaneous value $u_{cr}>u_c>u_{acr}$, namely during the time t_0 to t_1, the switch S_1 and S_4 both switch off. The inductor current i_2 flows through diode D_2 (the diode which is paralleled the switch S_2 inversely) and S_3 which is always open in the positive half-cycle. During the time $(t_1,t_2]$, u_{acr} is greater than u_c, so the switch S_1 turns on and the inverter is in the active state that i_2 flows through S_1 and S_3. The next duration is the same as that of $(t_0,t_1]$. In the duration of $(t_3,t_4]$, the instantaneous value u_c is greater than those of u_c and u_{acr} and the switch S_3 is closed. So the inverter is in the shoot-through state. The current i_2 flows through D_2 and S_3 while the power is exchanged between the passive components C_1 and L_1 (and also between C_2 and L_2) through S_3 and S_4 in this state. The simplified operation-mode figure (in positive cycle) is shown in Fig. 3 [16].

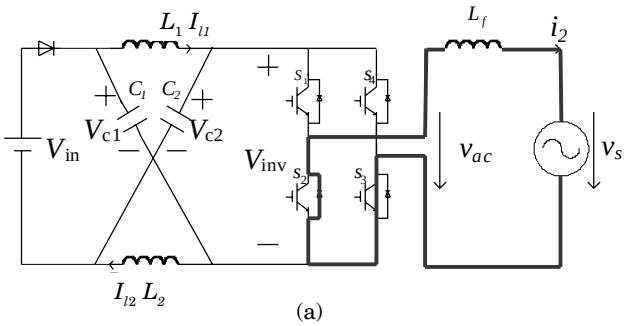

(a)

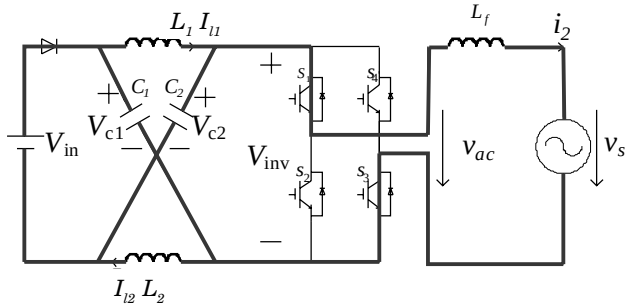

(b)

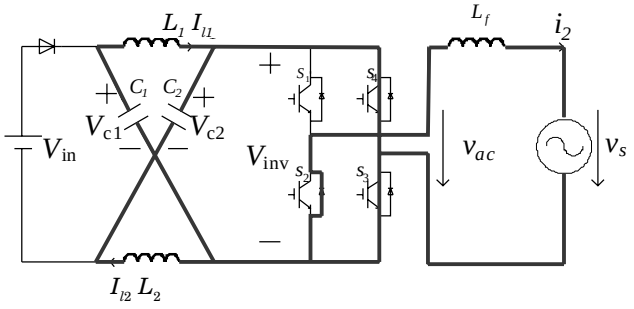

(c)

Fig. 3. The simplified operation modes in positive cycle (a)zero state (t_0,t_1]& (t_2,t_3], (b)active state(t_1,t_2], (c)shoot-through state(t_3,t_4]

From the symmetry circuits with $C_1=C_2$, $L_1=L_2$ in Fig. 1, we have the capacitor voltage $V_{c1}=V_{c2}$ and the inductance current $I_{l1}=I_{l2}$. It is given that the duty cycle of shoot-through state is d during a switching cycle, one has [6]

$$V_{inv} = \frac{1}{1-2d} V_{in} = BV_{in} \tag{1}$$

where

$$B = \frac{1}{1-2d} \tag{2}$$

$$V_c = \frac{1-d}{1-2d} V_{in}. \tag{3}$$

From Eqs.(1) and (3), when the shoot-through state exists, it has two working regions: one is $d \in [0, 1/2)$ and the other is $d \in (1/2, 1]$. According to Eq. (1), only when $d \in [0, 1/2)$, $V_{inv}>0$ is ensured. So the value of d must be limited in the range of $d \in [0, 1/2)$.

Equation (4) is obtained from Eqs. (1) and (2):

$$V_c = \frac{V_{in} + V_{inv}}{2}. \tag{4}$$

As to the single-phase inverter, its output voltage is

$$v_{ac} = MV_{inv} = BMV_{in} \tag{5}$$

where M is the modulation index of inverter.

Due to the relationship between the shoot-through state and the active state, the maximal value of M cannot exceed 1-d. From Eq. (5), one has

$$v_{ac} = BMV_{in} \le (1-d) \cdot \frac{1}{1-2d} V_{in} = V_c. \tag{6}$$

So, when the system is connected with the grid, the voltage V_c must be greater than $|v_{ac}|$peak, otherwise it will cause the current distortion even inverting failure.

3. MPPT design

In order to ensure the SCAs to output maximum power, a P&O MPPT method is introduced in the paper. The control figure is shown in Fig. 4. In Fig. 4, I_k and V_k are the momentary current and voltage respectively and I^* and V^* are the previous

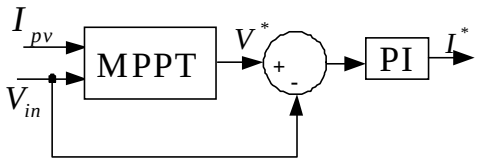

(a)

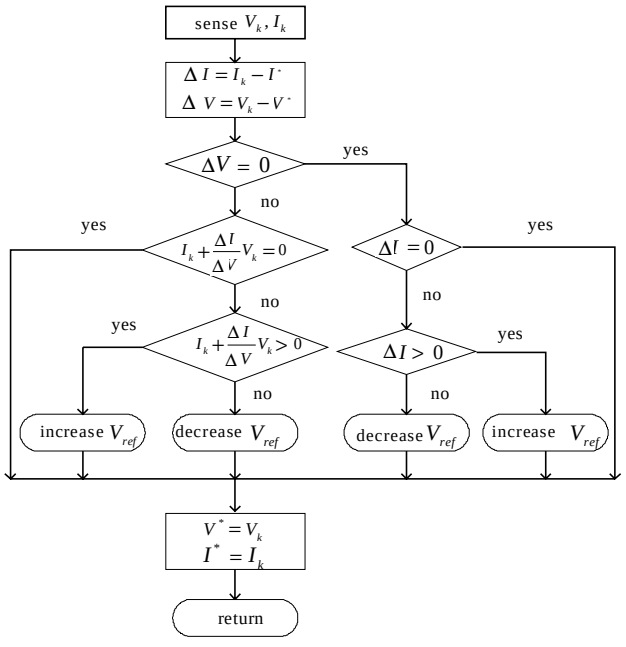

(b)

Fig.4. The MPPT controller (a) the controller configuration of the proposed system. (b) Flowchart of the MPPT method

current and voltage respectively while Ipv is the output current of the SCAs. Another control aim of MPPT is to obtain the current controller command $I_{2ref} = I^* \cdot \sin \omega t$, where I^* is obtained from a PI adjustment of the MPPT controller output

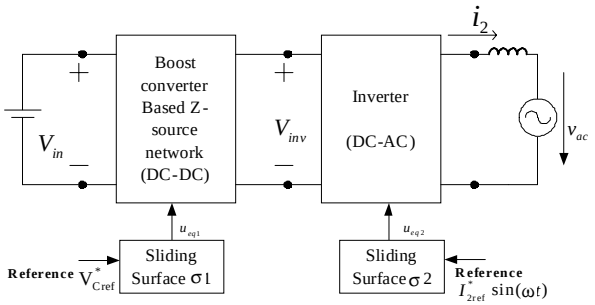

Fig. 5. Proposed sliding-mode controllers

(shown in Fig. 4a). The detailed description can be seen in the reference [17].

4. Controller design

Due to the shoot-through state, the DC-bus voltage of Z-source is the high-frequency pulse signal which is difficult to test. The capacitor voltage V_c, which is a constant voltage signal, is easy to test and control. According to Eq. (6), at the same time, the quality of output current can be better by controlling V_c. Because four devices of the inverter bridge must obey some special control logical rules, the paper presents two constant-frequency sliding-mode controllers to control the capacitor voltage of Z-source and the grid-connected current. The control variables of the controller are u_{cr} and u_{acr}, which are obtained from the equivalent control of the SMCs. And these two variables are compared with a high-frequency sawtooth signal to obtain the pulses controlling these devices. It is simple to obey the control rules by using the proposed control methods, meanwhile the advantages of the fast response and robustness of sliding-mode are retained.

The grid can be considered as an ideal voltage source. Two unattached close-loop controllers, shown in Fig. 5, are employed to control the voltage of Z-source capacitors and

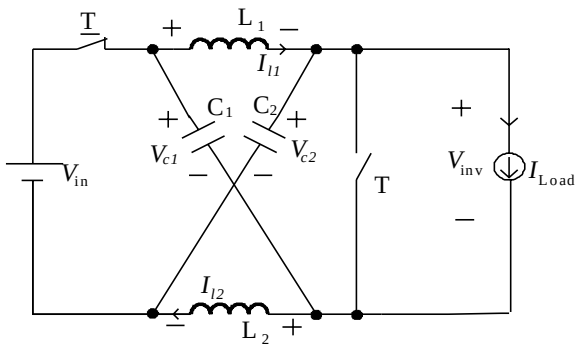

Fig. 6. Equivalent circuit with controlled DC side voltage

the grid-connected current. Not only the control destination is reached, but also the control rules are simplified.

4.1. DC side voltage controller. According to Fig. 1, the inverter can be equivalent to a current source (see Fig. 6). Considering $V_{c1}=V_{c2}=V_c$ and $I_{l1}=I_{l2}=I_l$, Eq.(7) can be established. In Fig. 5, **T** is off while **T** is on and **T** is on while **T** is off.

$$\begin{bmatrix} \dot{x}_1 \\ \dot{x}_2 \end{bmatrix} = \begin{bmatrix} \dfrac{2x_2 - V_{in}}{\mathrm{L}} \\ \dfrac{-2x_1 + I_{load}}{\mathrm{C}} \end{bmatrix} u_1 + \begin{bmatrix} \dfrac{-x_2 + V_{in}}{\mathrm{L}} \\ \dfrac{x_1 - I_{load}}{\mathrm{C}} \end{bmatrix} \tag{7}$$

where $X = [x_1 \quad x_2]^T = [I_l \quad V_c]^T$;

$$u_1 = \begin{cases} 1 & \text{T switch on} \\ 0 & \text{T switch off} \end{cases}.$$

The control aim is to get $x_2 \to x_2^*$ in the DC-side controller, and based on the two points that error items are replaced by state variables and the integral component of the reference's error is introduced, the sliding surface is chosen as

$$\sigma_1(x,t) = \mathrm{k}_1 x_1 + \mathrm{k}_2 x_2 + \mathrm{k}_3 \int_0^t (x_2 - x_2^*)\mathrm{dt} \ (\mathrm{k}_1, \mathrm{k}_2, \mathrm{k}_3 \neq 0) \tag{8}$$

where x_2^* is the reference value of x_2.

The switching law is chosen as

$$u_1 = \begin{cases} 0 & \text{when} \quad \sigma_1 > 0 \\ 1 & \text{when} \quad \sigma_1 \leq 0 \end{cases}. \tag{9}$$

Then Eq. (10) is obtained from Eq. (8)

$$\dot{\sigma}_1(x,t) = \mathrm{k}_1 \dot{x}_1 + \mathrm{k}_2 \dot{x}_2 + \mathrm{k}_3 (x_2 - x_2^*) = 0. \tag{10}$$

Assume that

$$\mathrm{sgn}(\sigma_1) = \begin{cases} 1 & \text{if} \quad \sigma_1 > 0 \\ -1 & \text{if} \quad \sigma_1 \leq 0 \end{cases} \tag{11}$$

and substitute (7) into (10):

$$\dot{\sigma}_1(x,t) = \mathrm{k}_1 \left[\left(\frac{-x_2 + V_{in}}{\mathrm{L}} \right) + \left(\frac{2x_2 - V_{in}}{\mathrm{L}} \right) u_1 \right] + \mathrm{k}_2 \left[\left(\frac{x_1 - I_{load}}{\mathrm{C}} \right) + \left(\frac{-2x_1 + I_{load}}{\mathrm{C}} \right) u_1 \right] + \mathrm{k}_3 (x_2 - x_2^*) \tag{12}$$

The equivalent control can be obtained

$$u_{eq1} = \frac{-\mathrm{k}_1 \mathrm{C}(V_{in} - x_2) + \mathrm{k}_2 \mathrm{L}(x_1 - I_{load}) + \mathrm{k}_3 \mathrm{LC}(x_2 - x_2^*)}{\mathrm{k}_1 \mathrm{C}(V_{in} - 2x_2) + \mathrm{k}_2 \mathrm{L}(2i_1 - I_{load})} \tag{13}$$

where u_{eq1} is continuous and belongs to [0, 0.5).

Deriving from Eqs.(12) and (9), one has

$$\lim_{\sigma_1\to 0^-}\frac{d\sigma_1}{dt}\overset{u_1=1}{=\!=}\lim_{\sigma_1\to 0^-}\left[k_1\frac{x_2}{L}-k_2\frac{x_1}{C}+k_3(x_2-x_2^*)\right]. \quad (14)$$

It is reasonable to consider that $x_2 - x_2^*$ is very small in the vicinity of the sliding surface. And x_1 and x_2 is greater than zero according to the limitation of $d \in [0, 1/2)$.

If $\frac{k_1}{L}V_{c\min}-\frac{k_2}{C}I_{l\max}>0$, one has

$$\lim_{\sigma_1\to 0^-}\frac{d\sigma_1}{dt}|_{u_1=1}>0. \quad (15)$$

In the same way Eq. (16) can be obtained

$$\lim_{\sigma_1\to 0^+}\frac{d\sigma_1}{dt}\overset{u_1=0}{=\!=}\lim_{\sigma_1\to 0^+}\left[k_1\frac{V_{in}-x_2}{L}+k_2\frac{x_1-I_{load}}{C}+k_3(x_2-x_2^*)\right]. \quad (16)$$

Equation (3) and the limitation $d \in [0, 1/2)$ $V_{in} - x_2 < 0$ is satisfied, and (x_1-I_{load}) is the value of the current i_c. In the vicinity of the sliding surface, the value of the voltage x_2 is very close to the voltage reference x_2^*. So the charging current of the capacitor i_c is very small. The inequality (17) can be concluded as follows:

$$\lim_{\sigma_1\to 0^+}\frac{d\sigma_1}{dt}|_{u_1=0}<0, \quad (17)$$

and the reaching condition is verified as follows.

1) If the representing point (RP) of the system is in the region where $\sigma_1 > 0$ and on the assumption that the RP cannot reach the sliding surface, the switch **T** is always on according to Eq. (9). So, d_{min} equals to zero and V_{in} equals to V_c, and I_l equals I_{load} according to Eq. (3). One has

$$\lim_{t\to\infty}\frac{d\sigma_1}{dt}\Big|_{\sigma_1>0}=\lim_{t\to\infty}\left[k_1\frac{-V_c+V_{in}}{L}+k_2\frac{I_l-I_{load}}{C}+k_3\left(V_{in}-x_2^*\right)\right]=\lim_{t\to\infty}k_3\left(V_{in}-x_2^*\right). \quad (18)$$

If $k_3 > 0$, then Eq. (18) is minus.

2) If the RP of the system is in the region where $\sigma_1 < 0$ and on the assumption that RP cannot reach the sliding surface, the switch **T** is off and its maximum duty is 0.5 according to the limitation of $d \in [0, 1/2)$. V_c will be infinite according to Eq. (3). One has

$$\lim_{t\to\infty}\frac{d\sigma_1}{dt}\Big|_{\sigma_1<0}=\lim_{t\to\infty}\left(\frac{k_1}{L}x_2-\frac{k_2}{C}x_1+x_2-x_2^*\right)$$

$$\left\|_{\frac{k_1}{L}V_{c\min}-\frac{k_2}{C}I_{l\max}>0}>\lim_{t\to\infty}x_2\right|_{\frac{k_1}{L}V_{c\min}-\frac{k_2}{C}I_{l\max}>0}>0. \quad (19)$$

Inequality (20) can be confirmed by Eqs. (15), (17), (18) and (19). So, Eq. (8), the sliding-mode surface, is existing and reachable.

$$\begin{cases}\dot\sigma_1<0 & \text{when } \sigma_1>0\\ \dot\sigma_1\ge 0 & \text{when } \sigma_1\le 0\end{cases}. \quad (20)$$

The close-loop system on the sliding surface can be obtained with the substitution of (7) into (10).

$$\begin{bmatrix}\dot x_1\\ \dot x_2\end{bmatrix}=\begin{bmatrix}\dfrac{-k_2x_2I_{load}+k_2V_{in}x_1+k_3C(2x_2^2-2x_2x_2^*-x_1V_{in}+x_2^*V_{in})}{k_1}\\ \dfrac{k_1(-x_1V_{in}+I_{load}x_2)+k_3L(-2x_1+I_{load})(x_2-x_2^*)}{k_1C(V_{in}-2x_2)+k_2L(2x_1-I_{load})}\end{bmatrix}. \quad (21)$$

By assuming that the right side of Eq. (21) is equal to zero, the stable point of the equation is shown as follows:

$$\begin{bmatrix}x_1\\ x_2\end{bmatrix}=\begin{bmatrix}\dfrac{I_{load}x_2^*}{V_{in}}\\ x_2^*\end{bmatrix}=\begin{bmatrix}\alpha I_{load}\\ x_2^*\end{bmatrix}. \quad (22)$$

When introducing the perturbation around the operating point, the small-signal state-space equation is obtained as

$$\frac{d}{dt}\Delta x_i=\frac{1}{\Lambda}\left(A\Delta x_i+B\Delta V_{in}+C\Delta I_{load}+D\Delta x_2^*\right)\quad (i=1,2) \quad (23)$$

where $A=\begin{bmatrix}k_2V_{in} & -k_2I_{load}+2k_3Cx_2^*-k_3CV_{in}\\ -k_1V_{in} & (k_1\text{-}2k_3L\alpha+k_3L)I_{load}\end{bmatrix}$,

$$B=\begin{bmatrix}\alpha k_2I_{laod}\\ -k_1\alpha I_{load}\end{bmatrix},$$

$$C=\begin{bmatrix}-k_2x_2^*\\ k_1x_2^*\end{bmatrix},$$

$$D=\begin{bmatrix}-2k_3Cx_2^*+k_3CV_{in}\\ (2\alpha\text{-}1)k_3LI_{load}\end{bmatrix},$$

$$\alpha=x_2^*/V_{in}$$

$$\Lambda = \mathrm{k}_1\mathrm{C}(V_{in} - 2x_2^*) + \mathrm{k}_2\mathrm{L}(2\alpha - 1)I_{load}.$$

If the poles of matrix $\boldsymbol{A}$ of Eq. (23) are all in the left plane, the close-loop system is stable. So the inequality is concluded as follows.

$$\begin{cases} \mathrm{k}_1^2 + (\mathrm{k}_2 V_{in} + 2\mathrm{k}_3\mathrm{L}\alpha)^2 + 2\mathrm{k}_1\mathrm{k}_2(2I_{load} - 1)V_{in} + 4\mathrm{k}_1\mathrm{k}_3\left[\mathrm{C}V_{in}\left(V_{in} - 2x_2^*\right) - \mathrm{L}\alpha\right] < 0 \\ \left(-\mathrm{k}_1 - \mathrm{k}_2 V_{in} + 2\mathrm{k}_3 L\alpha\right)\left[\mathrm{k}_1\mathrm{C}\left(V_{in} - 2x_2^*\right) + \mathrm{k}_2\mathrm{L}I_{load}\left(2\alpha - 1\right)\right] > 0 \\ \dfrac{\mathrm{k}_1}{\mathrm{L}}V_{c\min} - \dfrac{\mathrm{k}_2}{\mathrm{C}}I_{I\max} > 0 \end{cases} . \quad (24)$$

According to the inequality (24), one can determine the range of the coefficients k_1, k_2 and k_3 and then choose appropriate values by a trade-off.

4.2. AC current-shaper controllers. According to Fig. 1, the equivalent circuit figure with AC-current output is shown in Fig. 7. Its state equation can be obtained as follows.

$$\frac{dx_3}{dt} = \frac{1}{\mathrm{L}_\mathrm{f}}(V_{dc}u_2 - u'_{ac}) \quad (25)$$

where $x_3 = i_2$,

$$u_2 = \begin{cases} 1 & \text{S switch on} \\ 0 & \text{S switch off} \end{cases} .$$

The sliding surface σ_2 can be chosen as follows:

$$\sigma_2(x_3) = g\left(x_3 - x_3^*\right) + \int_0^t (x_3 - x_3^*)dt \quad (26)$$

where x_3^* is the reference value of x_3.

Set

$$u_2 = \begin{cases} 0 & \text{when} \quad \sigma_2 > 0 \\ 1 & \text{when} \quad \sigma_2 < 0 \end{cases} \quad (27)$$

and the equivalent control can be obtained from Eq. (26).

$$u_{eq2} = \frac{(x_3^* - x_3)\mathrm{L}_\mathrm{f}}{\mathrm{g}V_\mathrm{dc}} + \frac{v'_{ac} + \mathrm{L}_\mathrm{f}\dot{x}_3^*}{V_\mathrm{dc}} . \quad (28)$$

The inequality $\sigma_2 \cdot \dot{\sigma}_2 \le 0$ can be proved simply by the same method from Section 4.1. For the sake of the length of paper this derivation is omitted.

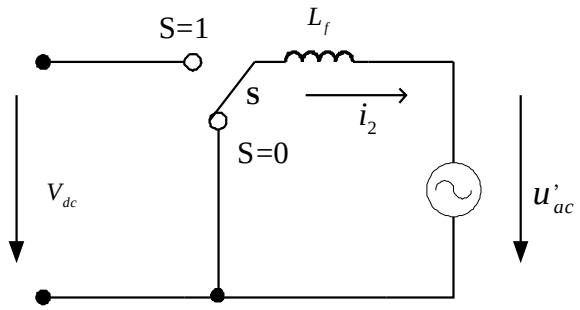

Fig. 7. Equivalent circuit with AC current output

5. Simulation and experiments

5.1. Simulation analysis. In the paper, the integrated single-phase single-stage grid-connected system is simulated. For simplification, a DC-voltage source replaces the SCAs in the simulation [1]. The static and dynamic simulation of the grid-connected system is presented in the paper. It includes three assumptions:

- Setting that V_{dc}=V_{Pv}, the working voltage of SCAs, is 100VDC and i_{out}, the output AC current, is 2.1A (rms), the voltage and current waveforms are shown in Fig. 8. The figures show the stable characteristic.
- The dynamic characteristic of the voltage control-loop is simulated based on the points, which are rated on condition that VP_v=V_{dc}=100V descend to V_{Pv}= V_{dc}=75V immediately and then back to V_{Pv}=V_{dc}=100V while iout is always 2.1A (rms). The voltage and current waveforms are shown in Fig. 9.
- The dynamic characteristic of the current control-loop is simulated and based on the points, which are rated on condition that i_{out}=2.1A(rms) descend to i_{out}=1.0A(rms) immediately and then back to i_{out}=2.1A(rms). The voltage and current waveforms are shown in Fig. 10. The grid-voltage is 110V (rms) in these assumptions.

We can conclude that the grid-connected current has low distortion, power factor is close to 1 and static voltage error of the capacitor of Z-source is small. (The reference value of the capacitor is 180V) from Fig. 8.

Figure 9 shows that when sudden changes of input voltage $\mathrm{V_{in}}$ burst, the tracking responses of the voltage of the Z-source are very fast. When the voltage changes from 100V to 75V, it takes about 12ms for the voltage to recover from the transient to the zero static-state error. And when the voltages changes from 75V to 100V, the time is about 8ms. Especially, while the input voltage steps up/down suddenly, the notch/protrusion following the over-shoot/ under-shoot of the Z-source output voltage is eliminated. These entire response features exhibit that the voltage controller has the good characteristics of the static and dynamic state that ensure the quality of the DC-side voltage and the grid-connected current.

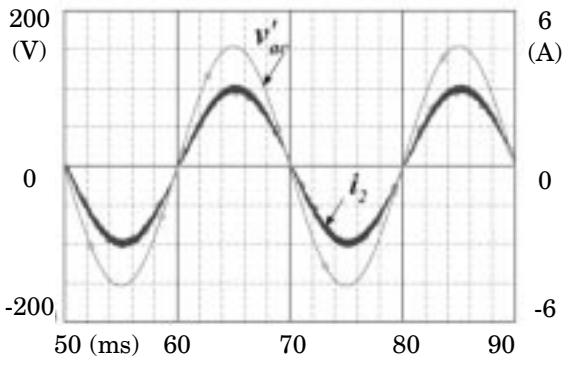

(a)

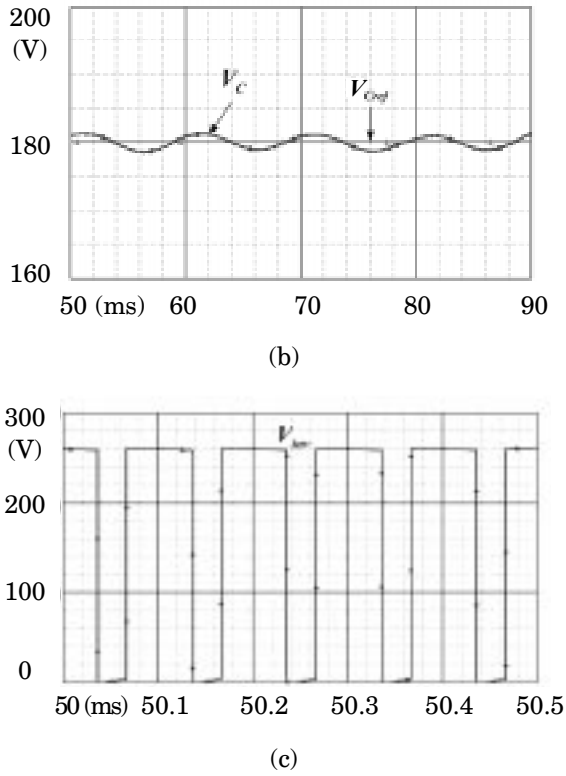

Fig. 8. Static waveforms (a) current and voltage waveforms of the grid (b) voltage waveform of the capacitor of Z-source and its reference (c) output voltage of Z-source

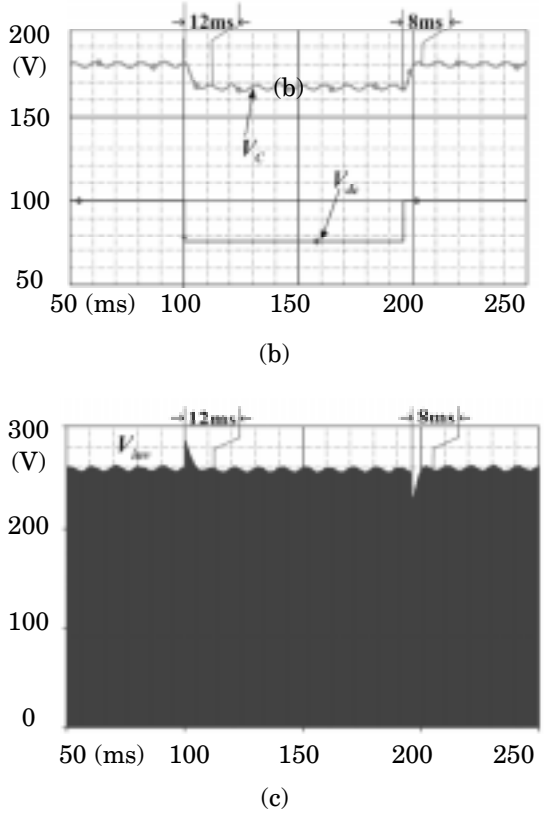

Fig. 9. Dynamic waveforms while V_{dc} changes (a) current and voltage waveforms of the grid, (b) voltage waveform of the capacitor of Z-source and input voltage V_{dc} (c) output voltage of Z-source

The excellent reference tracking is exhibited in Fig. 10 (a) when the grid-connected current reference changes suddenly. Figures 10 (b) and (c) show that the voltage fluctuates weakly due to the decoupled voltage and current control-loop and the static state and dynamic characteristics of the DC-side voltage.

The PV dynamic characteristic is that the working point of the output voltage and current of the SCAs will change at the same time when the irradiance amplitude changes rapidly. In order to make the simulation condition close to the practical condition, an approximative system with the PV dynamic characteristic is simulated. Two simulation conditions are presented as below:

- Set that $V_{dc}=V_{Pv}=100$V descend to $V_{Pv}= V_{dc}=75$V and then back to 95V in 20ms (one cycle of the grid) while i2 decreases from 2.1A(rms) to 1A in the duration.

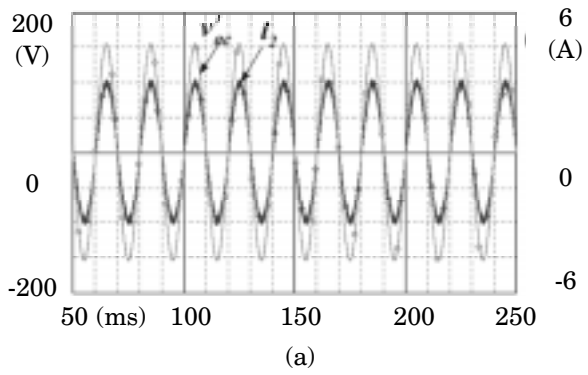

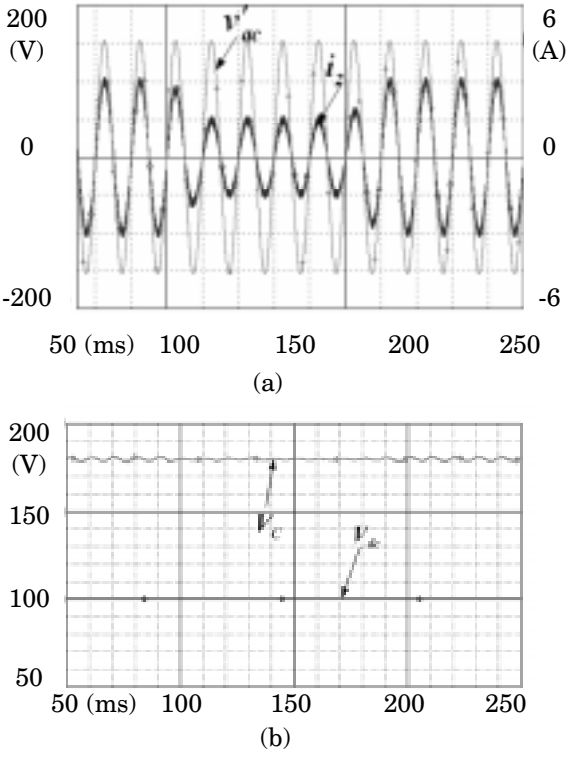

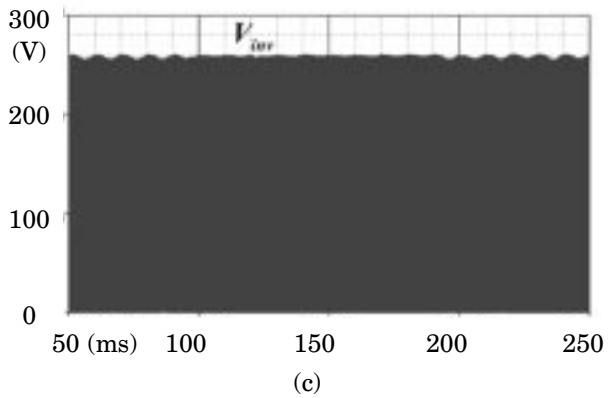

Fig. 10. Dynamic waveforms while i_2 changes (a) current and voltage waveforms of the grid, (b) voltage waveform of the capacitor of Z-source and input voltage V_{dc}
(c) output voltage of Z-source

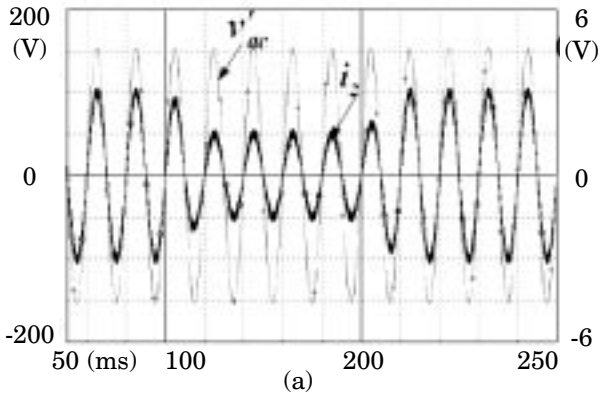

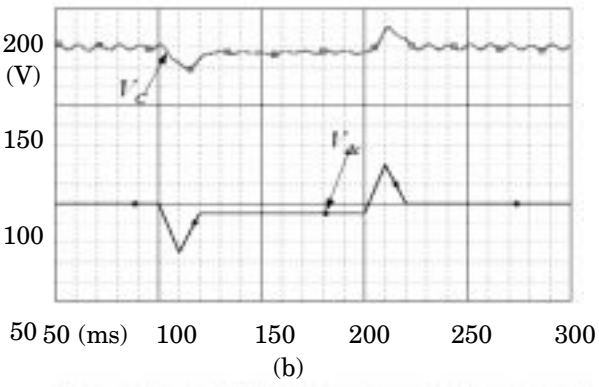

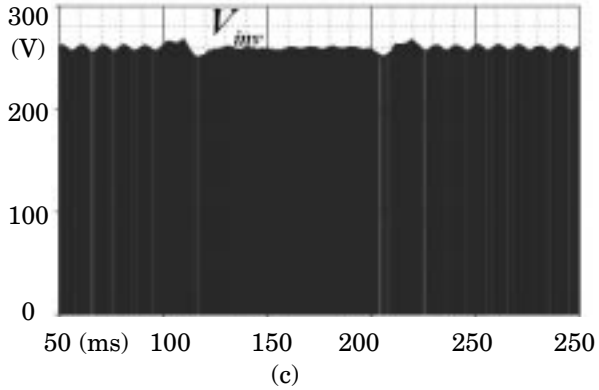

Fig. 11. Dynamic waveforms while V_{dc} and i_2 changes simultaneous (a) current and voltage waveforms of the grid, (b) voltage waveform of the capacitor of Z-source and input voltage V_d, (c) output voltage of Z-source

Table 1
Components value of the prototype and parameters of the controllers

components value of the prototype	Switch frequency	10k Hz
	Capacitor C_1&C_2	1000μF
	Capacitor C_{in}	1500μF
	Inductance L_1&L_2	1.0 mH
	Inductance L_f	12 mH
	Grid voltage v'_{ac}(rms)	110 V/50Hz
parameters of the controllers	Parameter of controller k_1	0.001
	Parameter of controller k_2	0.0015
	Parameter of controller k_3	1
	Parameters of controllers g	0.002

- Set that V_{dc}=V_{Pv}=95V rise to V_{Pv}= V_{dc}=120V and then back to 100V in 20ms while i2 increases from 1A(rms) to 2.1A in the duration. In these conditions the voltage and current control-loop operate simultaneously. The

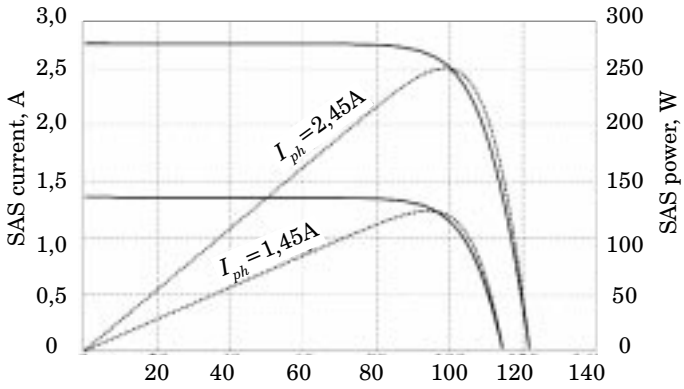

Fig. 12. Characteristics of the SAS while I_{ph}=2.5A and 1.25A (Line: *I-V* curve, dot line: *P-V* curve)

related waveforms are shown in Fig. 11.

5.2. Experiment analysis. To verify the performance of the proposed integral single-phase PV grid-connected system and its control arithmetic, an experimental

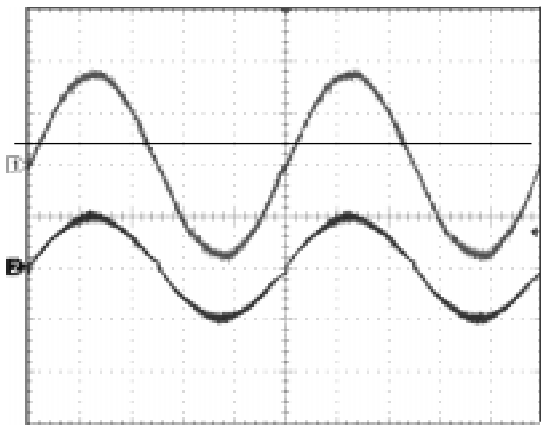

Fig. 13. Experimental grid-connected voltage and current while I_{ph}=2.5A. v'_{ac} (Ch1:85V/div), i_2 (Ch2: 1.5A/div) (Timebase: 4ms/div)

prototype is set up in the laboratory. The relative components value of the prototype and the parameters of the controllers are tabulated in Table 1. Besides a solar-array simulator (SAS) is used instead of the SCAs in the experiments. The SAS can simulate the *I-V* and *P-V* characteristic of some SCAs which are shown in Fig. 12.

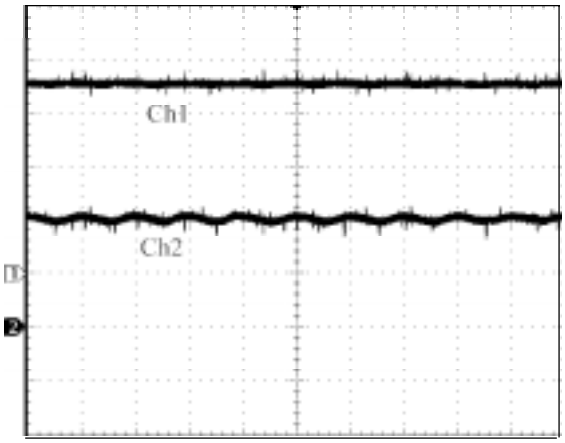

(a)

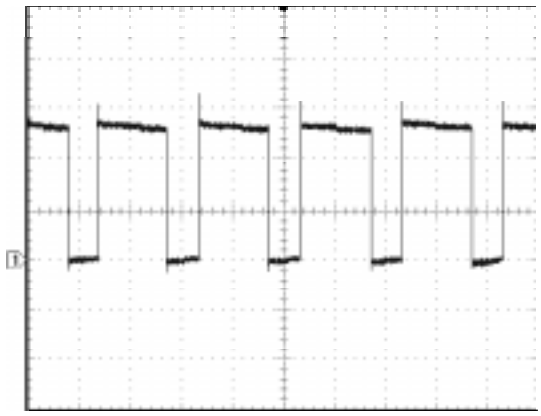

(b)

Fig.14 Experimental voltage and current waveforms while I_{ph}=2.5A, (a) V_c (Ch1:50V/div), V_{in} (Ch2:50*V*/div), (timebase: 10ms/div), (b) V_{inv} (Ch2:100*V*/div,timebase: 0.05ms/div)

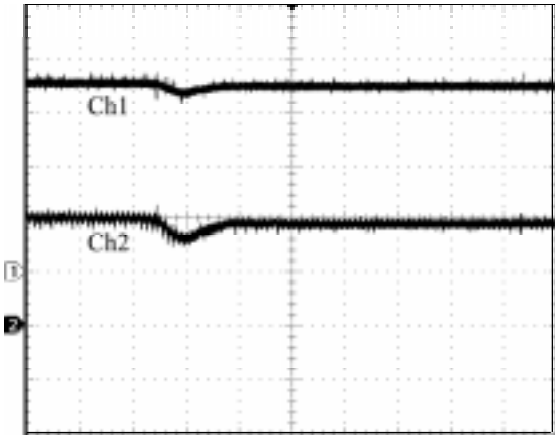

(a)

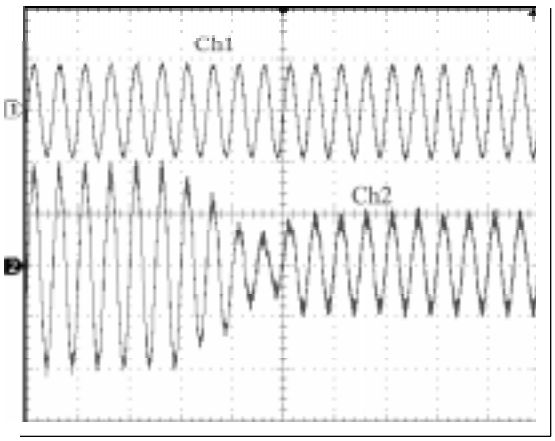

(b)

Fig. 15. Experimental voltage and current waveforms (I_{ph} is changed suddenly from 2.5A to 1.25A.) (a) V_c (Ch1:50V/div), V_{in} (Ch2:50*V*/div) (Timebase: 100ms/div), (b) v'_{ac} (Ch1:170V/div), i_2 (Ch2:1.5A/div) (Timebase: 40ms/div)

From the figure, the output maximum-power is 250W and the MPP retains 100V, while I_{ph}=2.5A and the output maximum-power is about 119W and the MPP keeps around 95V while I_{ph}=1.25A.

Figure 13 shows the waveforms the grid-connected voltage and current while the I_{ph} is equal to 2.5A. From the figure, one concludes that the current has such a low distortion that THD for the optimized controller was calculated to be 3.8% and high power factor is promoted. Next figure shows the voltage waveforms of Z-source, where Fig. 14(a) is V_{in} and V_c waveform and Fig. 14(b) is the output voltage V_{inv} waveform of the Z-source while I_{ph}=2.5A.

Figure 15 shows the voltage and current waveforms while Iph is changed suddenly from 2.5A to 1.25A. From Fig. 15(a), we can conclude that the voltage of the SAS first falls from 100V (the MPP of I_{ph}=2.5A) to around 75V in about 40ms and then return about 95V(the MPP of I_{ph}=1.25A) because of the MPPT arithmetic. Meanwhile, the grid-connected current also falls but there do not occur any distortions due to the effects of the two sliding controllers, especially the DC-side controller, that ensure the stabilization of the DC-bus voltage.

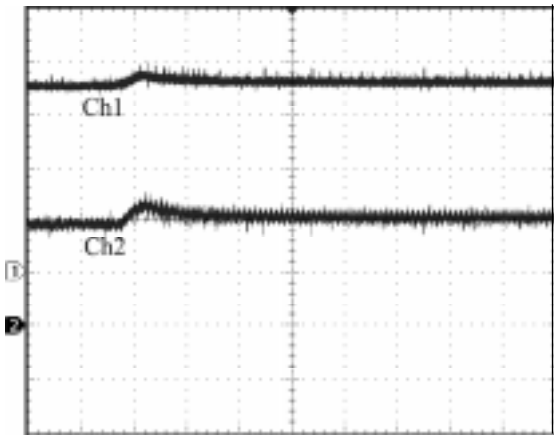

(a)

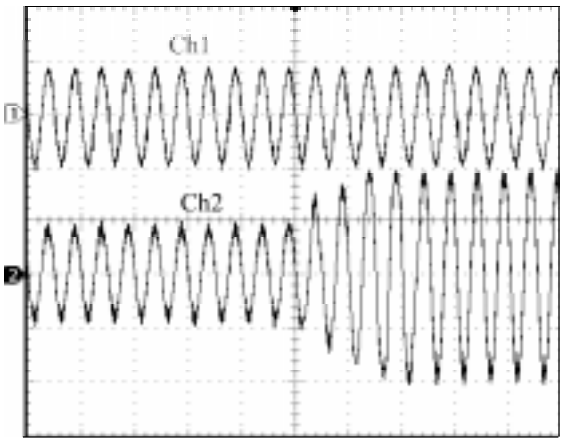

(b)

Fig. 16. Experimental voltage and current waveforms (I_{ph} is changed suddenly from 1.25A to 2.5A.) (a) V_c (Ch1:50V/div), V_{in} (Ch2:50V/div), (timebase: 100ms/div), (b) v'_{ac} (Ch1:170V/div), i_2 (Ch2:1.5A/div), (timebase: 40ms/div)

Figure 16 shows the voltage and current waveforms while Iph is changed suddenly from 1.25A to 2.5A.

6. Conclusions

The paper studies an integrated single-phase single-stage grid-connected inverter based on the Z-source which has three functional blocks to track the maximum power point, step-up/down voltage and output grid-connected current. According to the non-minimum-phase characteristic of Z-source impedance network and the functional demands of PV grid-connected system, two constant-frequency sliding-mode controllers with integral compensation are proposed to guarantee the system robustness. The effects caused by the non-minimum-phase characteristic are minimized. In the state of that the input voltage or the grid-connected current changes suddenly, any notches/protrusions following the over-shoot/under-shoot of the DC-bus voltage are eliminated. These excellent static-state and dynamic attributes of the SMCs ensure the quality of the grid-connected current. Furthermore, this method to control the DC-side voltage of the Z-source might also shed a light on other Z-source inverter/rectifier systems. Besides, a small-signal modelling method is employed to analyze the close-loop system to prove the system stability. At last, the simulation and experiment results show the proposed PV grid-connected inverter is feasible and the validity of the proposed control scheme is also confirmed.

Acknowledgements. We are grateful to Dr. Huajun Yu, an engineer of Shanghai Power Transmission&Distribution Co. Ltd., for his valued assistance and comments in this study. We also wish to thank Prof. Pengsheng Ye and Dr. Sanbo Pan who give their hands to this study.

References

[1] B.M.T Ho and H. Shu-Hung Chung, "An integrated inverter with maximum power tracking for grid-connected PV systems", *IEEE Trans. Power Electronics* 20(4), 953-962 (2005).

[2] M. Meinhardt, T. O'Donnell, and et al., "Miniaturized low profile module integrated converter for photovoltaic applications with integrated magnetic components", IEEE *Appl. Power Electronics Conf. and Exposition*, 305-311 (1999).

[3] M. Calais, J. Myrzik, and et al., "Inverters for single-phase grid connected photovoltaic systems-an review", *33rd Annual IEEE Power Electronics Specialists Conf.*,1995-2000 (2002).

[4] Y.T. Tan, D.S Kirschen, and et al., "A model of PV generation suitable for stability analysis", *IEEE Trans. Energy Conversion* 19(4), 748-755 (2004).

[5] L.B. Wu, Z.M Zhao, and et al. "Modified MPPT strategy applied in single-stage grid-connected photovoltaic system", *Proc. Int. Conf. Electrical Machines and Systems,* 1027-1030 (2005).

[6] F.Z. Peng, "Z-source inverter", *IEEE Trans. Industry Applications* 39(2), 504-510 (2003).

[7] F.Z. Peng, M.S. Shen, and K. Holland, "Application of Z-source inverter for traction drive of fuel cell-battery hybrid electric vehicles", *IEEE Trans. Power Electronics* 22(3), 1054-1061 (2007).

[8] F.Z. Peng, X.M. Yuan, and et al., "Z-source inverter for adjustable speed drives", *IEEE Power Electronics Letters* 1(2), 33-35 (2003).

[9] C.J. Gajanayake, D.M.Vilathgamuwa, and C.L. Poh, "Small-signal and signal-flow-graph modeling of switched Z-source impedance network", *IEEE Power Electronics Letters* 3(3), 111-116 (2005).

[10] C.L. Poh, D.M. Vilathgamuwa, and C.J. Gajanayake, "Transient modeling and analysis of pulse-width modulated Z-source inverter", *IEEE Trans. Power Electronics* 22(2), 1498-507 (2007).

[11] C.J. Gajanayake, D.M. Vilathgamuwa, and C.L. Poh, "Modeling and design of multi-loop closed loop controller for Z-source inverter for Distributed Generation", *IEEE Power Electronics Specialists Conference*, 1-7 (2006).

[12] J.W. Jung, M. Dai, and A. Keyhani, "Modeling and control of a fuel cell based Z-source converter", *IEEE Applied Power Electronics Conference and Exposition*, 1112-1118 (2005).

[13] J.H. Lee, P.E. Allaire, and et al., "Integral sliding-mode control of a magnetically suspended balance beam: analysis, simulation, and experiment", *IEEE/ASME Trans. Mechatronics* 6(3), 338-346 (2001).

[14] Y. He, and F.L. Luo, "Sliding-mode control for dc-dc converters with constant switching frequency", *IEEE Proc.: Control Theory and Application* 153(1), 37-45 (2006).

[15] C.C. Marouchos, *The Switching Function: Analysis of Power Electronic Circuits,* The Institution of Electrical Engineering, London, 2006.

[16] M.S. Shen and F.Z. Peng, "Operation modes and characteristics of the Z-source inverter with small inductance", *Industry Applications Conference,* 1253-1260 (2005).

[17] Y.C. Kuo, T.J. Liang, and J.F. Chen, "Novel maximum-power-point-tracking controller for photovoltaic energy conversion system", *IEEE Trans. Industrial Electronics,* 48(3), 594-601 (2001).